Design and Radiation Hardness of Next Generation Solar UV Radiometers

Samuel Gissot, Ali BenMoussa, Boris Giordanengo, Ali Soltani, Terubumi Saito, Udo Schühle, Udo Kroth, and Alexander Gottwald

***Abstract*-- For next space-based ultraviolet (UV) solar radiometers, we propose a design based on subsystem components that are selected according to lessons learned from previous flying missions and ground irradiation campaigns. UV interference filters inherited from space-based solar missions show strong degradation caused by structural changes that lead to an important decrease of visible light rejection. Wide bandgap semiconductors (WBGS) are used for the photodetectors: innovative metal–semiconductor–metal (MSM) based on Aluminum Nitride (AlN) and Diamond-based PIN photodetectors were developed, characterized and compared to the commonly used silicon photodiode technology (AXUV and SXUV types). Insignificant degradation of the WBGS based-photodetector performances were observed after exposure to protons of 14.4 MeV energy showing a good radiation tolerance up to fluences of $1x10^{11}$ p+/cm^2. Onboard calibration strategy based on UV LEDs are used as well to distinguish the detector's drift from inevitable degradations of the optical front filters.**

I. Introduction

To withstand environmental conditions in near-Earth and interplanetary space for several years (typically 10 years), next generation ultraviolet (UV) radiometers for space applications must be light, compact, and robust to space radiation. Robustness to space radiation environment is crucial to extend the stability of the radiometric calibration of UV solar missions.

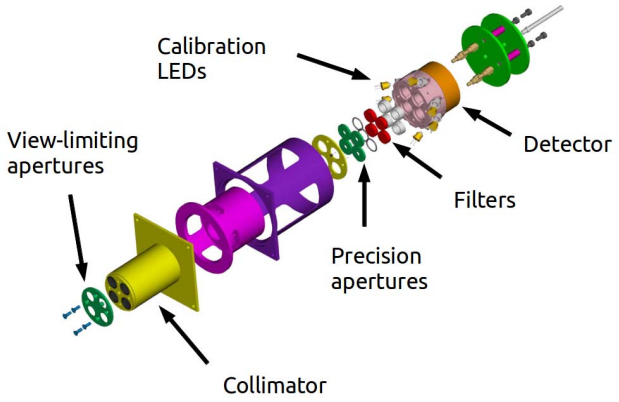

Fig. 1: Schematic representation of a solar UV radiometer (4 spectral channels) showing the precision aperture, the filter, the photodetector, and the onboard calibration LEDs.

A robust design for next-generation solar UV radiometers for space-based observations is proposed which results from our research activities on wide bandgap materials (WBGM). The optical design is based on a combination of apertures, a filter and a photodetector: the solar flux is spatially filtered by an entrance and a precision apertures, then spectrally selected by UV interference filter before being collected by a photodetector as shown in Fig. 1. The generated photocurrent is then amplified and converted into a voltage and digitized by an Analog-to-Digital converter. This design is directly inherited from the PROBA2/LYRA instrument [1] and shall be re-used in future foreseen missions (such as ESIO and PICASSO CubeSat). A redundant radiometer concept is also proposed to maximize the accuracy and the reliability of the measurements and for eventual correction of the measured data.

Radiation hardness against protons (p^+) is a primary concern for space-based instruments during long-period interplanetary orbits or when flying in low-Earth orbit and exposed to the inner protons belt, especially because of the South Atlantic Anomaly (SAA) [2]. Proton irradiation test results of radiometer filters, UV photodetectors, and onboard calibration LEDs in order to address their performance in space environment. On this basis, we define a reliable design baseline for the next generation of UV solar radiometers.

Manuscript received July 11, 2014-. The authors acknowledge the support of BELSPO through PRODEX fundings.

S. Gissot, A. BenMoussa, and B. Giordanengo are with the Royal Observatory of Belgium (ROB), Brussels, Belgium (telephone: +3223730237, e-mail: samuel.gissot@oma.be).

A. Soltani is with Institut d'Electronique, de Microélectronique et de Nanotechnologie (IEMN), Villeneuve d'Ascq, France.

T. Saito is with the Department of Environment and Energy, Tohoku Institute of Technology, Sendai, Miyagi, Japan.

U. Schühle is with Max Planck Institute for Solar System Research, Justus-von-Liebig-Weg 3, D-37077 Göttingen, Germany.

A. Gottwald and U. Kroth are with Physikalisch-Technische Bundesanstalt (PTB), Abbestr. 2-12, D-10587 Berlin, Germany.

II. Redundant Design For Space-based Radiometer

The redundancy concept i.e. the combination of similar independent radiometer units was successfully implemented on LYRA/PROBA2 and PREMOS/PICARD, where two units are read in parallel to inter-calibrate their spectral channels. The unit that is used to monitor continuously the sun can be corrected by comparing the measured irradiances to those obtained by other units that are less exposed to the sun.

Each radiometer unit contains at least two individual detection channels necessary to reconstruct the salient features of the solar spectral irradiance in the UV as recommended in [3] such as Herzberg (197-237 nm) and Lyman-α (116-126 nm) channels.

A door mechanism is needed to measure the photodetector dark current (DC) and to correct the science data acquisition. Moreover, UV instruments are particularly sensitive to surface contamination that can polymerized when exposed later to solar radiation [11]. In this context, the door is crucial to protect the instrument especially during on-ground test activities.

Finally, onboard calibration light-emitting diodes (LEDs), ideally two different ones per channel, are used to monitor the responsivity degradation of the photodetector and to disentangle aging of the photodetector from the optical filter.

III. Effects of Proton-irradiation

Interference filters, photodetectors, and LEDs were irradiated with protons at the Light Ion Irradiation Facility at Louvain-La-Neuve, Belgium (cyc.ucl.ac.be). The irradiations were performed in air and at normal incidence of the proton beam geometry. The energy spectrum was centered at 14.4 MeV with a flux of $1x10^8$ p^+/cm/s, the nearest energy to the one specified in the Space Environment Information System (SPENVIS.oma.be), i.e., 10 MeV-equivalent fluence to predict the 10-year mission fluence of 10^{11} p^+/cm^2 under 1 mm Al shielding for solar mission in a sun-synchronous low-Earth orbit at altitude of 725 km (such as in the case of PROBA2 spacecraft). To take into account uncertainties in the model, we applied a radiation margin factor of 5. The optical measurements in the near UV (NUV) and visible range for filters and photodetectors were carried out at STCE/ROB (DeMeLab) facilities using a collimated and tunable monochromatic light beam emitted by 30 W deuterium (190 nm to 300 nm) and 100 W tungsten (300 nm to 1000 nm) light sources combined with a monochromator and a digital lock-in amplifier system. Absolute calibration was obtained using a Si photodiode calibrated at the National Institute of Standards and Technology (NIST) that was used as a reference detector. At lower wavelength range from 110 nm to 225 nm, measurements are carried out at the synchrotron radiation facilities of the Physikalisch Technische Bundesanstalt (PTB) in Berlin [4].

A. UV Interference Filters

UV filters used to select the Lyman-α (116 nm to 126 nm) and Herzberg (197 nm to 237 nm) wavelength passbands are based on Al/MgF_2 multilayers coatings (from Princeton Instruments) and were irradiated with 14.4 MeV proton beam at a fluence of 10^{11} p^+/cm^2.

Fig. 2 shows the spectral transmittance measurements before and after proton irradiation of the Herzberg and the Lyman–α filters. As observed, the transmission at peak wavelength decreases by approx. 7% for both filters. The bandwidth is not significantly affected, preserving the interference characteristics of the UV filters. However both filters were affected for wavelengths higher than 300 nm by the proton irradiation, which has strongly increased the filter transmission. As an example, in the visible – near-infrared (NIR) range the transmission has increased by a factor 2 for the Lyman–α filter and 3 to 5 for the Herzberg filter.

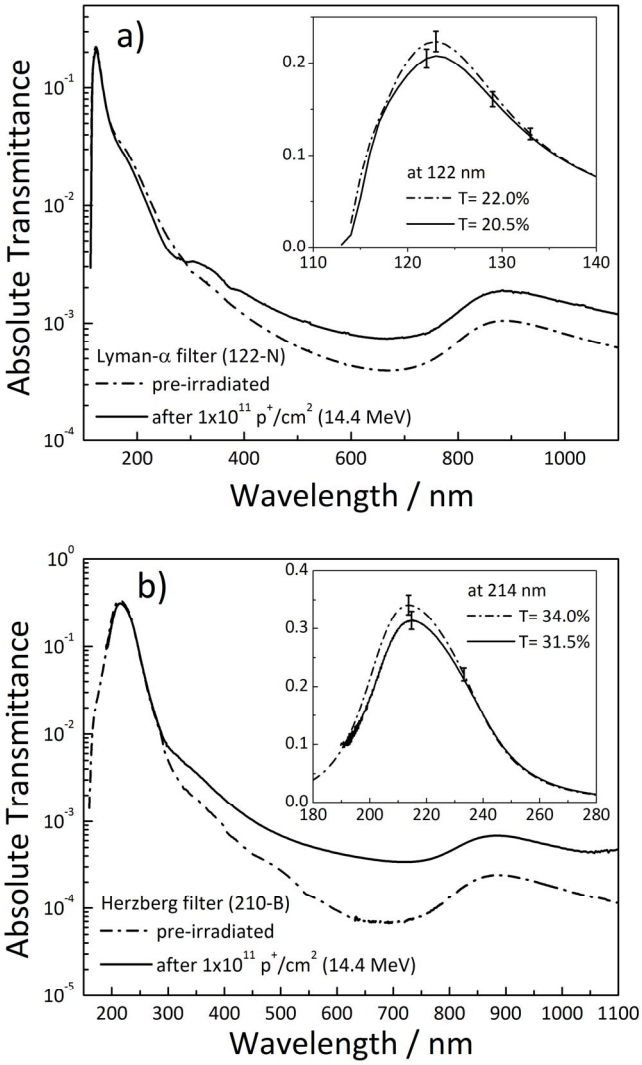

Fig. 2: Absolute transmittance of a) Lyman-α and b) Herzberg UV interference filters before and after (several weeks) proton irradiation.

As shown in Fig. 3, some cracks on the thin Al top layer and deformation in the multilayer structure have been observed by scanning electron microscopy (SEM) that could explain the increase of the transmission in the visible range and the small decrease of the peak transmission in the UV, respectively. It should be added that other NUV interference filters from different manufacturers were irradiated showing the same behavior, i.e., an increase of the out-of-band (visible)

transmission and negligible (below 5 %) decrease of its peak transmission in the UV range.

Deeper analysis and simulations together with low proton energy effects are still ongoing and is intended for a future publication.

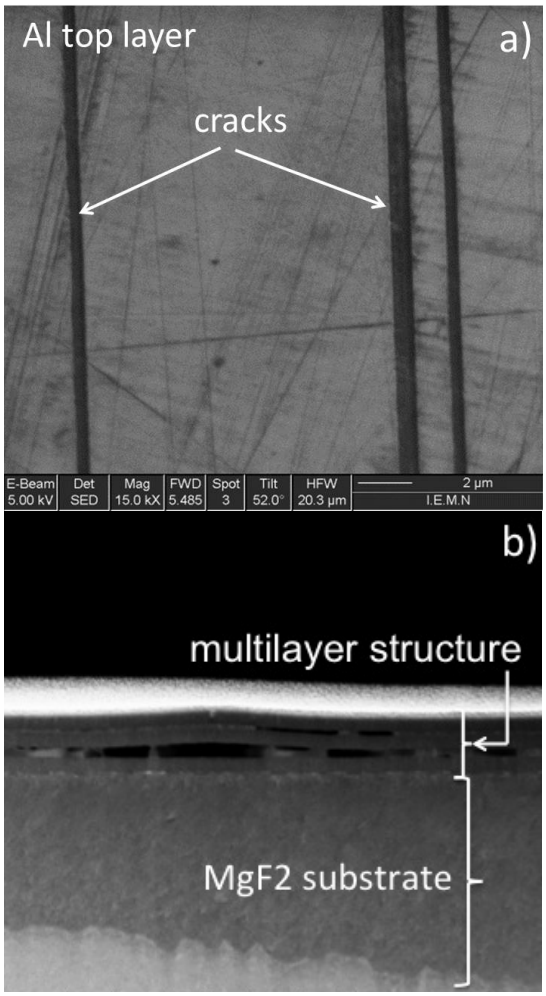

Fig. 3: SEM images of a) Lyman–α filter showing cracks on top coated layer and b) Herzberg filter cross-section by focused-ion-beam milling showing structural deformation (delamination) of its multilayer structure after 14.4 MeV proton irradiation (up to 10^{11} p^+/cm^2).

B. WBGM-based Photodetectors

Radiation effects at the detector level in relevant space environment is anticipated with the use of WBGM-based detectors which include Diamond and Aluminum Nitride (AlN) materials as promising alternatives to commonly used Silicon (Si) detectors. Diamond and AlN as the active layer make the detectors radiation-hardened to UV photons and energetic particles because of their high bandgap value.

Fig. 4: MSM-AlN photodetectors of several sizes (1.1 to 4.3 mm diameter).

In this study, metal-semiconductor-metal MSM-AlN (see Fig. 4), Diamond PIN, Si AXUV and SXUV photodiodes used here as a reference, were characterized in the 200 nm – 1100 nm spectral range before and after irradiation with 14.4 MeV proton beam at a fluence of 10^{11} p^+/cm^2. Results are shown in Figs. 5, 6, 7, and 8.

1) MSM-AlN Photodetectors

Measured just after the proton irradiations, the MSM-AlN dark current (DC) increases almost linearly with the proton fluence (not shown). However the increase of the DC resulting from the collisions with the incoming protons was annealed after two weeks at room temperature as shown in the inset of Fig. 5.

Fig. 5 shows the spectral response of the MSM-AlN in the 190 nm - 700 nm wavelength range. The peak UV photo-response and the spectral responsivity between 190 nm and 290 nm is not degraded after proton irradiation (within the error bar). However the sub-bandgap responsivity and specially above 550 nm seems to increase indicating possible bulk displacement damages with the introduction of new defect levels in the AlN bandgap structure. The visible light rejection ratio of 5 orders of magnitude between 200 nm and 550 nm is still preserved for UV solar observations.

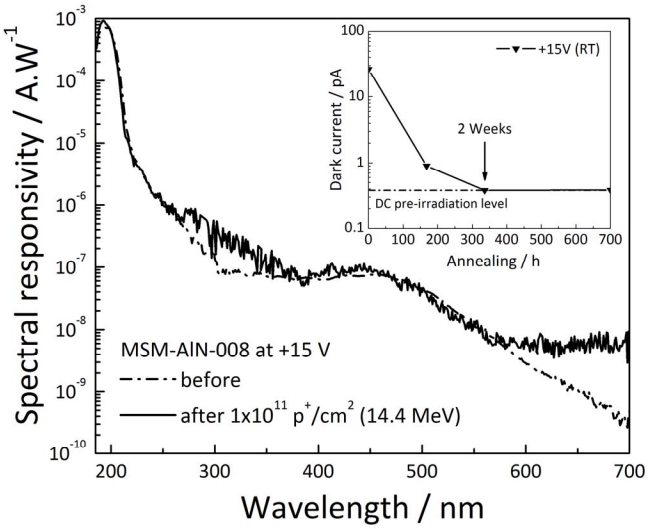

Fig. 5: Spectral response of the MSM-AlN photodetector after proton irradiation. Inset: dark current as a function of elapsed time at room temperature (RT) after irradiation.

2) Diamond PIN Photodiodes

The DC of PIN diamond photodiode as shown in the inset of Fig. 6 is increased by a factor 10 after the proton irradiation but it returns to its pre-irradiation level after one week of annealing at room temperature. The fact that the PIN photodiodes operate in unbiased mode, i.e., do not require an external voltage, implies a very low DC of approximately 10^{-14} A. Note that the diamond PIN photodiode has no native oxide and its surface is coated by a thin (3 nm to 5 nm) Al layer used as n-type contact layer.

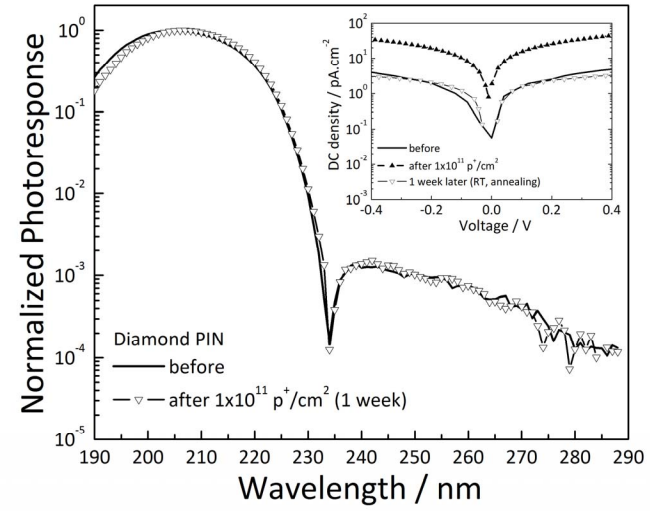

Fig. 6: Spectral response of the PIN Diamond photodiode after proton irradiation. Inset: dark current density at room temperature before and after irradiation.

Fig. 6 shows the spectral responsivity normalized to its maximum pre-irradiation value. The spectral responsivity of the PIN diamond around 200 nm remains more or less unaffected (uncertainties of 2 %). The diamond PIN photodiodes exhibit a high responsivity of 10 to 30 mA/W around 200 nm which is not degraded after proton irradiation [1]. However the sub-bandgap responsivity seems to be noisier around 270 nm but here the photoresponse signal is limited by the optical setup.

3) Reference Si Photodiodes

The Si n-on-p SXUV and AXUV types from Optodiode Corp. are used as reference and for comparison.

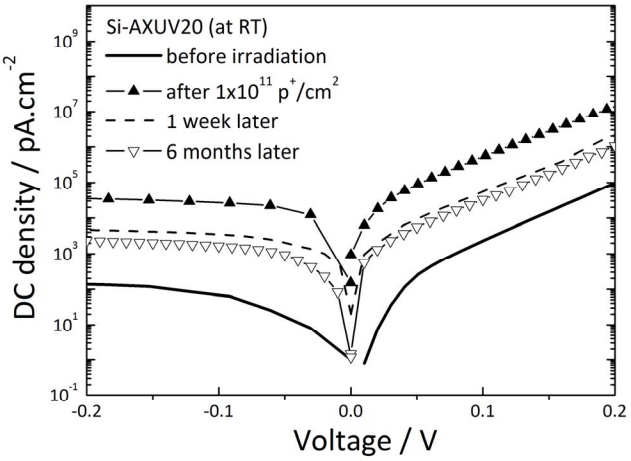

Fig. 7: Dark current density at room temperature before and after irradiation.

The DC of the Si-AXUV photodiode increases by a factor of 100 (from 0.3 pA to 30 pA) after irradiation when measured one week later as shown in Fig. 7. For statistical significance, three Si-AXUV photodiodes have been irradiated. The DC increase cannot be only attributed to the surface ionization damage induced by protons, which takes place generally at the Si–SiO_2 interface. Instead at the 14.4 MeV energy proton, the main contribution arises from displacement damage-induced DC from atomic Coulomb and inelastic / elastic nuclear interactions [6] leading to depletion (bulk) defects. Six months after irradiation, we measured that the DC remains higher than its pre-irradiation value (by approx. a factor 10), except in the zero bias case where the DC is fully recovered. However to minimize the leakage current, the Si-AXUV photodiodes should be operated at low temperature. On the other hand, the DC of the SXUV (not shown) is not affected by the irradiation and fully recovered after one-week annealing at room temperature.

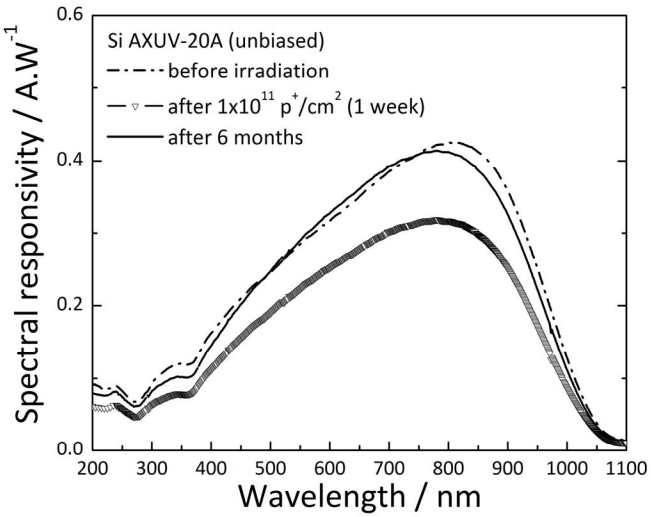

Fig. 8: Si AXUV spectral responsivity before and after proton irradiation.

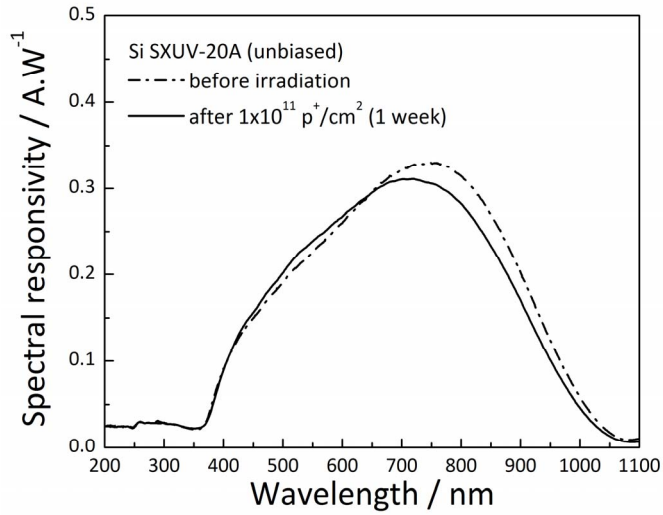

Fig. 9: Si SXUV spectral responsivity before and after proton irradiation.

As shown in Fig. 8, after proton irradiation the Si-AXUV photodiode responsivity significantly degrades (e.g., - 30 % at 835 nm in Fig. 8), indicating that the displacement damages (non-ionizing) is the dominant mechanism with the introduction of trap levels within the Si bandgap structure. We also observed at different frequencies (not shown), a variation of the capacitance-voltage characteristics of the Si-AXUV photodiode suggesting a change of the effective doping concentration. However optical measurements were repeated 6 months after irradiation, and as seen in Fig. 8 the spectral responsivity partially reached its pre-irradiation level although we observed a shift in the responsivity peak. Protons create both displacement damage but also ionization-induced damage along the $Si–SiO_2$ interface (trap states) that negatively affects the surface collection efficiency and consequently the responsivity which can recombine (anneal) with time at room temperature.

As shown in Fig. 9, the spectral responsivity in NUV-VIS of the Si-SXUV is slightly affected by the proton irradiation. The spectral responsivity in the range 1 nm to 240 nm was also measured for both photodiodes and shows no significant degradation in the EUV and VUV spectral ranges (not shown): this demonstrates that the AXUV and SXUV photodiodes are robust to 14.4 MeV proton energy up to $1x10^{11}$ p^+/cm^2 fluence. It should be mentioned that the better radiation tolerance of the Si-SXUV series photodiodes observed during the DC measurements is probably due to the metal-silicide front window used. The metal-silicide replaces the SiO_2 window of the Si-AXUV, thus eliminating the ionization exposure-induced instability [7] however for the price of significant lower UV spectral responsivity.

C. UV LEDS for On-board Detector Calibration

Onboard calibration UV-LEDs based on WBGM are used to assess the responsivity of the photodetectors in order to distinguish a detector's drift from degradations of the filters [8]. The LEDs are situated between the filter and detector, but outside the optical path of the sun as viewed by the detector through a precision aperture (see Fig. 1). Thus the LEDs only monitor the degradation of the detector and not the optical filters.

Several UV LEDs based on $Al_xGa_{1-x}N$ were irradiated:

- 250 nm, 315 nm, and 355 nm (SETI, AlGaN-based),
- 365 nm (NSHU551B, Nichia, GaN-based).

Three LEDs (for each type) were irradiated in an unbiased condition with all leads grounded. The LED characterizations were carried out using a mini-spectrometer (model USB4000-UV-VIS) and an integrating sphere. To reduce the measurement variability due to the sensitivity of LEDs to temperature, the mini-spectrometer was coupled to a temperature control module (model USB-TC).

Table 1 shows the comparative results of UV-LEDs (from SETI, USA) signal after proton irradiation at 14.4 MeV energy. It is demonstrated that their average wavelength (spectrum peak wavelength) $\lambda_{0.5m}$ and bandwidth $\Delta\lambda_{0.5m}$ are almost not affected by proton irradiation. The UV LEDs demonstrate a good radiation tolerance up to a fluence of $4x10^{11}$ p^+/cm^2.

TABLE I
AlGaN-based UV-LED degradation after proton irradiation (energy: 14.4 MeV, fluence: $4x10^{11}$ p^+/cm^2).

LED	S_p (%)	$\lambda_{0.5m}$ (nm)	$\Delta\lambda_{0.5m}$ (nm)	P (%)
@ 250 nm	-5.4	-0.091	-0.028	-5.4
@ 315 nm	-6.8	+0.13	+0.00	-6.7
@ 355 nm	-5.4	+0.18	+0.10	-4.8

However the maximum signal (Sp) and the integrated power (P) decrease slightly with the irradiation. Fig. 10 shows a peak signal loss (10%) that corresponds to an extreme case of 80 years in Low Earth Orbit (1 mm Al shielding, radiation margin factor of 5). This decrease is due to an increase of the non-radiative recombination centers within the LED active layer [9][10]. Details of the measurement results and analysis together with recommendations for future solar instruments using onboard LEDs are given in [9].

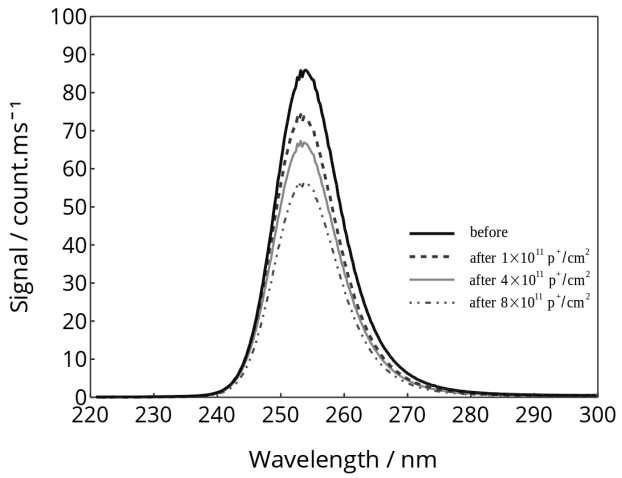

Fig. 10: AlGaN LED (@ 250 nm) emission spectra measured before and after 14.4 MeV proton irradiation at fluences of $1x10^{11}$, $4x10^{11}$ and $8x10^{11}$ p^+/cm^2 resp. corresponding to 10, 40 and 80 years of typical space proton environment in Low Earth Orbit.

IV. Conclusions

For the next generation of solar UV radiometers, rigorous cleanliness programs at instrument and spacecraft levels are required in order to prevent contamination effects. Indeed, the observed degradation on solar UV radiometers is mainly caused by the presence of contaminant species [11] on the optical front filter surface, which reduce the UV light transmission. Currently, there is no possibility of mitigating contamination in space once molecules have irreversibly settled after UV-polymerization, which is a classical concern for UV solar instruments. However methods such as a redundancy design concept should be implemented for tracking instrument degradation and complemented by other solar inter-calibration instruments.

Concerning the robustness of radiometer components to proton irradiation, our conclusions are the following:

1) UV interference filters show strong degradation with a decrease of the light rejection in the visible and NIR spectral range which prevents to use them in combination with visible light sensitive Si-based photodetectors,

2) On the other hand, WBGM-based detectors are the best candidates for spaceborne UV solar radiometer. By their nature, WBGM have a much lower thermally induced DC and are radiation-hard semiconductors, which significantly extend the stability of the instrument radiometric calibration. Thanks to their visible blindness, diamond and AlN photodetectors can also mitigate the effects of ongoing degradation of the filters due to particle impacts in space (e.g., pinholes, cracks). Their degradation in relevant proton environment is negligible an acceptable,

3) UV LEDs for onboard detectors calibration were irradiated and we could identify LEDs based on AlGaN materials as a good option.

V. References

[1] A. BenMoussa et al., "Pre-flight calibration of LYRA, the solar VUV radiometer on board PROBA2", *Astronomy and Astrophysics*, vol. 508, pp. 1085-1094, 2009.

[2] S. C. Freden and G. A.Paulikas, "Trapped Protons at Low Altitudes in the South Atlantic Magnetic Anomaly", *Journal of Geophysical Research*, vol. 69, pp. 1259, 1964.

[3] G. Cessateur, J. Lilensten, T. Dudok de Wit, A. BenMoussa, and M. Kretzschmar, "New observation strategies for the solar UV spectral irradiance", *J. Space Weather Space Clim.*, vol. 2, no. A16, 2012

[4] A. Gottwald, U. Kroth, M. Richter, H. Schoeppe, and G. Ulm, "Ultraviolet and vacuum-ultraviolet detector-based radiometry at the Metrology Light Source", *Measurement Science and Technology*, vol. 21, no. 12, pp. 125101, 2010.

[5] A. BenMoussa, A. Soltani, J.-C. Gerbedoen et al., "Developments, characterization and proton irradiation damage tests of AlN detectors for VUV solar observations", *Nuclear Instruments and Methods in Physics Research B*, vol. 312, pp. 48-53, 2013.

[6] I. Jun, M. A. Xapsos, S. R. Messenger, E. A. Burke, R. J. Walters, G. P. Summers, and T. Jordan, "Proton nonionizing energy loss (NIEL) for device applications", *IEEE Trans. Nucl. Sci.*, vol. 50, pp.1924 -1928, 2003.

[7] R. Korde, C. Prince, D. Cunningham, R. E. Vest, and E. Gullikson, "Present status of radiometric quality silicon photodiodes", *Metrologia*, vol. 40, no. 1, pp.145, 2003.

[8] B. Giordanengo, S. Gissot, and A. BenMoussa, "Characterization and Irradiation Damage Tests of AlGaN UV LEDS for Detector Spaceborne Calibration", International Symposium on Reliability of Optoelectronics for Systems (ISROS), Toulouse, France, 16 - 20 June 2014.

[9] A. Johnston, "Radiation effects in light-emitting and laser diodes", *IEEE Transactions on Nuclear Science*, vol. 50, pp. 689, 2003.

[10] O. Pursiainen, N. Linder, A. Jaeger, R. Oberschmid, and K. Streubel, "Identification of aging mechanisms in the optical and electrical characteristics of light-emitting diodes", *Applied Physics Letters*, vol. 79, pp. 2895, 2001.

[11] A. BenMoussa, S. Gissot, U Schühle., et al, "On-Orbit Degradation of Solar Instruments", *Solar Physics*, vol. 288, pp. 389-434, 2013.